# Fabrication and characterization of two-dimensional cubic AlN photonic crystal membranes containing zincblende GaN quantum dots

**Sarah Blumenthal**[*,1], **Matthias Bürger**[1], **Andre Hildebrandt**[2], **Jens Förstner**[2], **Nils Weber**[1], **Cedrik Meier**[1], **Dirk Reuter**[1], **and Donat J. As**[1]

[1] University of Paderborn, Department of Physics, Paderborn, Germany
[2] University of Paderborn, Department of Theoretical Engineering, Paderborn, Germany

[*] Corresponding author: e-mail sarah.blumenthal@upb.de

We successfully developed a process to fabricate freestanding cubic aluminium nitride (c-AlN) membranes containing cubic gallium nitride (c-GaN) quantum dots (QDs). The samples were grown by plasma assisted molecular beam epitaxy (MBE). To realize the photonic crystal (PhC) membrane we have chosen a triangular array of holes. The array was fabricated by electron beam lithography and several steps of reactive ion etching (RIE) with the help of a hard mask and an undercut of the active layer. The r/a- ratio of 0.35 was determined by numerical simulations to obtain a preferably wide photonic band gap. Micro-photoluminescence (μ-PL) measurements of the photonic crystals, in particular of a H1 and a L3 cavity, and the emission of the QD ensemble were performed to characterize the samples. The PhCs show high quality factors of 4400 for the H1 cavity and about 5000/3000 for two different modes of the L3 cavity, respectively. The energy of the fundamental modes is in good agreement to the numerical simulations.

**1 Introduction** Group-III nitride QDs are well-suited for optical and quantum optical devices, operating in the ultraviolet spectral range, because of their wide bandgap and their capability to operate at high temperatures [1]. In particular, micro-resonators allow to control the spontaneous emission of light and to realize an efficient single photon emitter (SPE) [2]. Promising candidates for such devices are PhC nanocavities, because high high quality factors ($Q$) are achievable [3, 4].

Recently, SPE employing hexagonal QDs in AlN were already realized [5]. However, hexagonal GaN (h-GaN) QDs exhibit the Quantum Confined Stark Effect caused by strong internal electric fields along the c-axis. These fields lead to a spatial separation of the maxima of the wave functions of electron and holes and therefore to a reduced recombination probability of electrons and holes in confined states [6]. To maybe overcome this issue we have made use of c-AlN/c-GaN heterostructures as a starting material for PhC fabrication. Due to the cubic crystal structure, internal polarization fields do not appear and the maxima of the wave functions of electrons and holes are no longer separated. Hence, we expect a higher recombination probability.

Two-dimensional (2D) photonic crystals with a refractive index contrast in the vertical direction allow the confinement of light in all three dimensions. The refractive index contrast is attained by an undercut of the active layer. The optical cavity is realized by a controlled defect in the PhC. Very high quality factors were observed for h-AlN/GaN QDs [7].

In this paper, we investigate H1 and L3 PhC membranes. Both cavities are based on a triangular lattice of air holes. The triangular lattice is preferred over the square lattice due to the larger photonic band gap for this symmetry. Additionally, the triangular lattice requires a lower refractive index contrast to generate a photonic band gap [8].

Phys. Status Solidi C **13**, No. 5–6 (2016)

293

The H1 cavity is marked by one missing hole in the center of the PhC, the L3 cavity by three missing holes arranged in a linear fashion (see Fig. 2(a) and Fig. 2(b)). Simulations have been performed to show the tuning behavior of the PhC by varying the radius of the air holes and to verify the experimental results using the commercially available time domain solver of CST Microwave Studio [9]. The PhCs are optically characterized by micro-photoluminescence measurements at room temperature. We demonstrate high Q factors of 4400/5000 for the H1/L3 cavity, respectively.

**2 Experimental** The substrate is a 10 µm thick 3C-SiC layer on top of 500 µm Si (001) substrate (see Fig**.** 1). Our samples are grown by plasma-assisted molecular beam epitaxy. The active layer consists of 60 nm c-AlN. We have successfully implemented self-assembled c-GaN QDs in Stranski-Krastanov growth mode in the c-AlN matrix [10]. These samples act as a basis for the fabrication of 2D PhC membranes. The coupling of the QDs to the resonance mode should increase the rate of spontaneous emission [11].

The challenge is the fabrication of the membranes. Because of the short emission wavelength of the material, the dimensions of the PhC have to be very small (hole size between 50 and 120 nm, lattice constant between 100 and 200 nm).
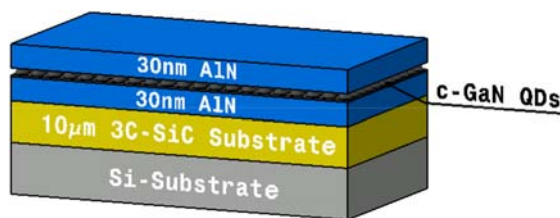


**Figure 1** Cubic GaN QDs created by the Stranski-Krastanov mode, embedded in a 60 nm c-AlN matrix. The growth was performed by plasma-assisted molecular beam epitaxy on 10 µm 3C-SiC (001) substrate on top of 500 µm Si.

To fabricate the PhC membranes, a 60 nm $SiO_2$ hard mask is deposited on top of the active layer by plasma enhanced chemical vapor deposition. This hard mask ensures the protection of the active layer during the following etching steps. After spin coating of positive photoresist (ZEP520A), a triangular array of holes is patterned by electron beam lithography. This pattern is transferred to the hard mask by reactive ion etching (RIE) using $CHF_3$ (20 sccm) and Ar (20 sccm). Afterwards, the photoresist is removed with the help of oxygen plasma. In the next step, the active layer is etched by RIE, applying $SiCl_4$ (4.5 sccm) and Ar (4.5 sccm) as process gases.

Subsequently, the hard mask is removed by using a buffered oxide etching solution and finally the AlN/GaN is underetched (see Fig. 2(d)). Conventionally, this step is done by wet chemical etching. Unfortunately, it is not possible to etch 3C-SiC nitrides by wet chemical etching, without chemically attacking the active layer. For this rea-

son we used RIE at a temperature of 375 °C with $CF_4$ (90 sccm) as process gas to realize the free standing membrane.

**3 Results and discussion**
**3.1 Scanning electron microscopy**
Figures 2(a) and (b) show a top view SEM image of a H1/L3 PhC membrane after all fabrication steps. From these images, the performance of the etching process can be evaluated. The air holes have a perfectly circular shape. The radius of the holes is d = 50 nm (± 1 nm) and the lattice constant is a = 170 nm (± 2 nm).
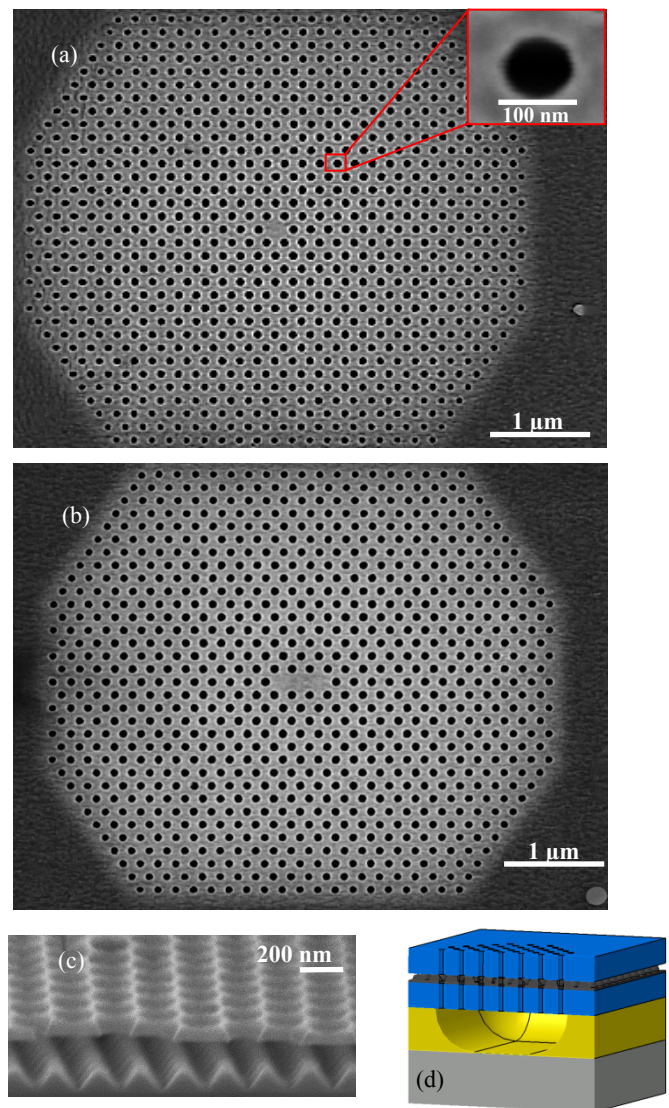


**Figure 2** Top view SEM image of a H1 (a) and L3 (b) PhC membrane and close-up image of one air hole. (c) Cross-section of a photonic crystal membrane to check the undercut. (d) Schematic structure of the PhC.

Only the radii of the holes show some decrease of about 3-5 nm at the border of the PhC. This is due to the proximity effect during electron beam lithography. In

Fig. 2(c) a cross section of a PhC is shown to demonstrate the suspended membrane. The sample is tilted 82° with respect to the substrate holder. A sawtooth-like profile of the etched 3C-SiC is clearly visible. Therefore, the underetching depth varies from about 150 nm to about 300 nm. We assume that this underetching depth and the high roughness of the 3C-SiC layer ensure a decoupling of the optical mode from the substrate. The surface roughness of the AlN layer is measured with atomic force microscopy measurements (AFM) in a $10 \times 10 \ \mu m^2$ field. An rms surface roughness of 8.4 nm is determined, which originates mainly from the last etching step by RIE.

**3.2 Simulations** Figures 3(a) and (b) show the dispersion relations for a triangular array of holes. These numerical simulations were done using the three-dimensional finite integration technique. TE-like as well as TM-like modes were simulated. For the simulation a refractive index for c-AlN of $n_{AlN} = 2.19$ [12] and for c-GaN of $n_{GaN} = 2.73$ [13] at 3.5 eV were assumed. The light cone is





**Figure 3** Photonic band structure of (a) TE-like modes and (b) TM-like modes for a slab thickness of 59 nm and r/a = 0.35. The black line indicates the light cone. (c) Lattice in real space and the corresponding lattice in reciprocal space with the first Brillouin zone. The high symmetry-points at the corners of the irreducible Brillouin zone are shown (shaded grey).

indicated by the black line [14]. For TE-like modes a photonic band gap, over all symmetry points below the light cone, exists. For TM-like modes no photonic band gap occurs. Figure 3(c) shows the lattice in real space and the corresponding lattice in reciprocal space with the first Brillouin zone. An air filling factor r = 0.32a and a lattice constant of a = 170 nm are chosen to obtain a preferably wide photonic band gap. These parameters were determined experimentally and used for both, H1 and L3 cavity simulations. The photonic band gap of TE-like modes extends from 0.46 c/a to 0.51 c/a (with c the velocity of light). This results in a gap of 371 meV. Obtaining a wide photonic band gap is challenging due to the relatively low difference of the refractive index of AlN compared to air.

**3.3 Micro-photoluminescence measurements**
The optical properties of the PhC were studied by micro-photoluminescence (μ-PL) measurements at room-temperature. A HeCd laser with a peak wavelength of 325 nm was used as excitation source. The incident power of the laser beam was about 6 mW. The laser was focused on the sample (beam diameter 2 μm) and the photoluminescence signal collected with a spectrometer (entrance slit 20 μm, focal length 500 mm) with a CCD detector. For the measurement of the QD ensemble a grating was used with 150 lines/mm blazed at a wavelength of 500 nm and a spectral resolution of 1 meV at 3.7 eV. The measurements of the PhCs were done with a grating of 1200 lines/mm (blaze wavelength 500 nm) and the maximal resolution of 0.4 meV.
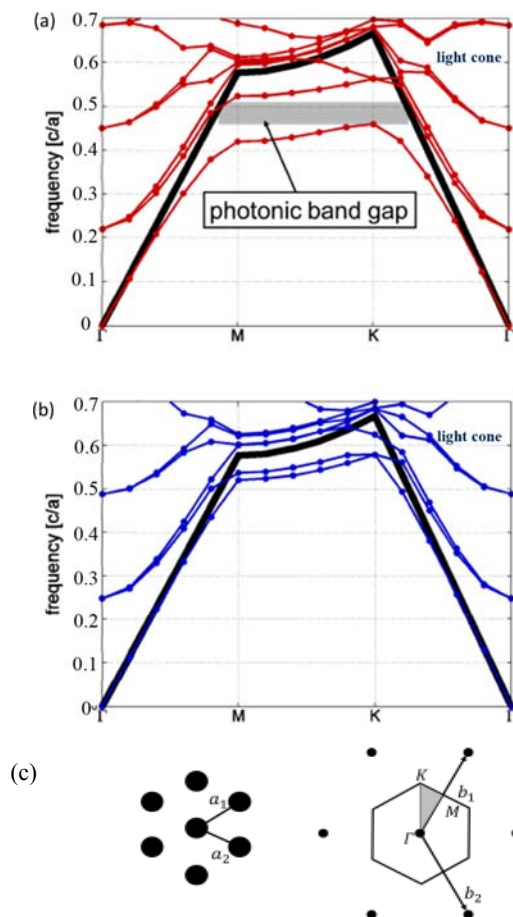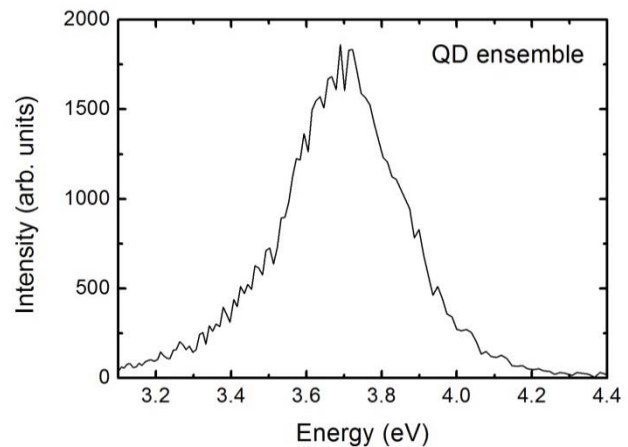


**Figure 4** Spectrum of the QD ensemble before fabrication of the PhC.

In Fig. 4 a spectrum of a non-patterned c-AlN/c-GaN sample is displayed. The peak emission is at 3.7 eV. It shows a superposition of the emission bands of many individual QDs. A broad full width half maximum (FWHM) of about 360 meV is observed. The broadening of the peak results from the size distribution of the QDs. This broad size distribution is shown in the AFM image in Fig. 5. The meas-

Phys. Status Solidi C **13**, No. 5–6 (2016)

295

ured sample consists of uncapped c-GaN QDs on top of a 30 nm c-AlN layer. An area size of $500 \times 500$ nm$^2$ was measured and a density of quantum dots of about $1.2 \cdot 10^{11} \frac{QDs}{\text{cm}^2}$ is determined.



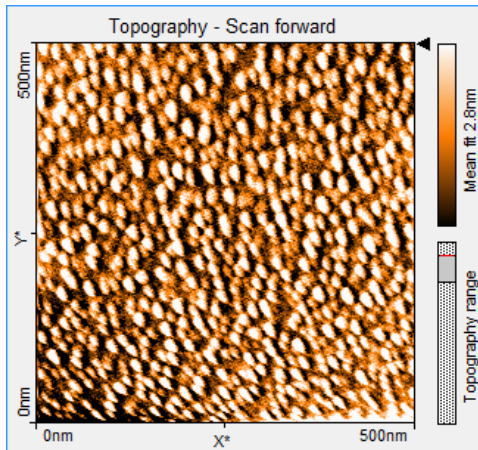**Figure 5** AFM image of uncapped c-GaN QDs grown on 30 nm AlN.
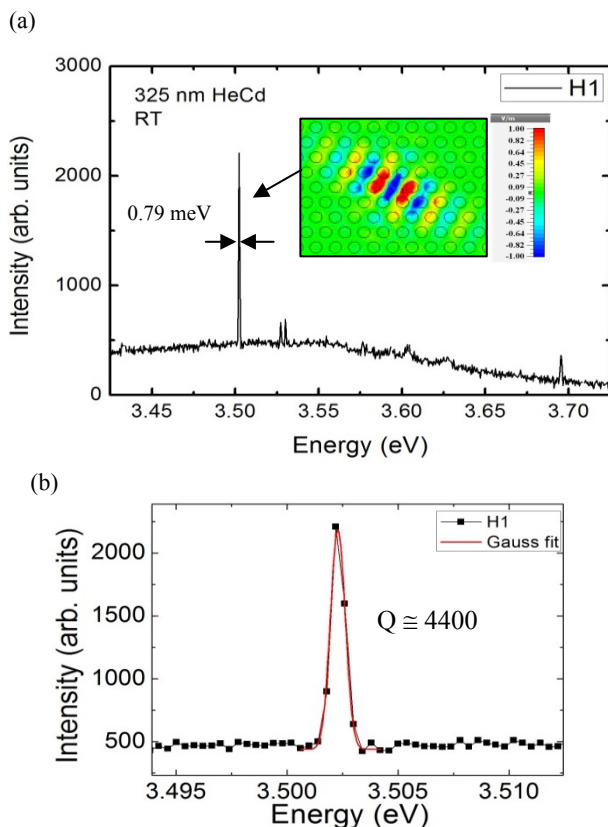
(a)



(b)



**Figure 6** Experimental room temperature spectrum of a H1 cavity (a). Inset: electric field distribution ($E_y$) of the fundamental mode and related color-scale normalized to 1. (b) Close-up and Gaussian fit of the fundamental mode.

The sample, shown in Fig. 4, was applied to fabricate different PhC membranes. The following parameters were used for the PhC: hole diameter r = 50 nm, lattice constant a = 170 nm and slab thickness h = 59 nm.

After processing, μ-PL measurements at room temperature were performed on several H1 and L3 PhCs. In Fig. 6 and Fig. 7 the μ-PL measurements of one of these H1 and L3 cavities are presented, respectively.
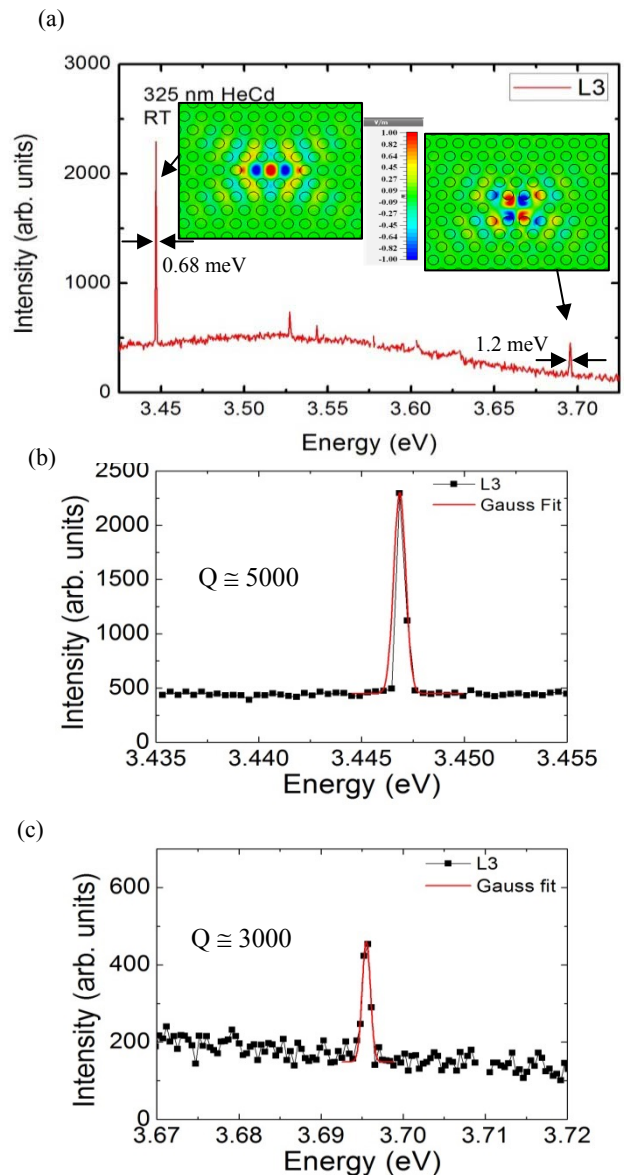
(a)



(b)



(c)



**Figure 7** Experimental room temperature spectrum of a L3 cavity (a). Inset: electric field distribution ($E_y$) of the defined modes and related color-scale normalized to 1. (b) and (c) close-up and Gaussian fit of the modes.

In these spectra distinct modes are observed. The spectrum of the H1 cavity (see Fig. 6(a)) is dominated by the mode at 3.51 eV. This mode has a FWHM of ΔE = 0.79 meV and a corresponding quality factor of about 4400 (see

Fig. 6(b)). For this fundamental mode, the electric field distribution of the field in y-direction is depicted in the inset. The additional peaks near 3.525 eV are due to residual plasma lines of the HeCd-laser.

The spectrum of the L3 cavity (see Fig. 7(a)) shows two narrow peaks at 3.45 eV and 3.69 eV. The fundamental mode at 3.45 eV dominates the spectrum. It shows a FWHM of $\Delta E = 0.68$ meV (see Fig. 7(b)), which is in the range of the resolution of our setup. Additionally, it contains only four measured data points. For that reason we estimated the quality factor to a value of about $Q = \frac{E}{\Delta E} \cong 5000$ (compare extended spectral range in Fig. 7(b)). This quality factor is comparable to the maximal quality factor for this material system, which was simulated in Ref. [15].

A higher order mode (shown in Fig. 7(c)) is situated at a peak energy of 3.7 eV. The linewidth of $\Delta E = 1.2$ meV corresponds to a quality factor of about $Q \cong 3000$. The associated electric field distributions in y-direction are again plotted as insets in Fig 7(a) for both L3 modes.

To validate the experimental results simulations using the time domain solver of CST Microwave Studio were performed. Table 1 shows the mode energies determined experimentally (see Fig. 6 and Fig. 7) and calculated by simulations. The mode energies of the fundamental modes of the H1 and L3 cavities are contrasted to each other demonstrating an excellent agreement between experiment and simulation.

The small difference between the experimental and the simulated values can be explained by imperfections of the photonic crystal, for example as described in Section 3.1, by the decrease of the hole radius from the center to the border due to the proximity effect. As discussed in Ref. [15], the hole radius and the lattice constant are very sensitive parameters for the Q factor of the fundamental mode. The other peaks visible in the spectrum of Fig. 7(a) are again caused by plasma lines from our HeCd laser, which could not be suppressed completely.

**Table 1** Mode energy for experimental and simulated modes in H1 and L3 cavities.

| cavity | mode energy (exp.) [eV] | mode energy (sim.) [eV] |
|---|---|---|
| H1 | 3.51 | 3.52 |
| L3 | 3.45 | 3.46 |
|  | 3.7 | 3.68 |

**4 Conclusions** In summary, a patterning process is successfully applied to fabricate c-AlN PhC membranes on 3C-SiC substrate. The active layer consists of c-GaN QDs, grown by molecular beam epitaxy in Stranski-Krastanov growth mode, embedded between two 30 nm c-AlN layers. The fabrication process contains a structuring step with electron beam lithography to realize the triangular lattice of holes and multiple steps of RIE etching. We have investigated the optical properties of the QD ensemble and of different PhC membrane nanocavities. The QD ensemble shows a broad FWHM of 360 meV. Two PhC structures were realized, including H1 and L3 cavities, to compare their spectral properties. It was observed that both nanocavities show fundamental modes with high quality factors. For the H1 cavity a quality factor of about 4400 was observed and for the fundamental mode of the L3 cavity a quality factor of about 5000 was estimated. The experimental and simulated mode energies of the fundamental modes differ only by an energy shift of 10 meV. This small difference can be explained by imperfections of the PhC.

**References**
[1] J.F. Muth, J.H. Lee, I.K. Shmagin, R.M. Kolbas, H.C. Casey, B.P. Keller, U.K. Mishra, and S.P. DenBaars, Appl. Phys. Lett. **71**, 2572 (1997).
[2] S. Laurent, S. Varoutsis, L. Le Gratiet, A. Lemaître, I. Sagnes, F. Raineri, A. Levenson, I. Robert-Philip, and I. Abram, Appl. Phys. Lett. **87**, 163107 (2005).
[3] A. Badolato, K. Hennessy, M. Atatüre, J. Dreiser, E. Hu, P.M. Petroff, and A. Imamoglu, Science **308**, 1158 (2005).
[4] E.M. Purcell, Phys. Rev. **69**, 681 (1946).
[5] S. Kako, C. Santori, K. Hoshino, S. Götzinger, Y. Yamamoto, and Y. Arakawa, Nature Mater. **5**, 887 (2006).
[6] C. Santori, S. Götzinger, and Y. Yamamoto, Appl. Phys. Lett. **87**, 051916 (2005).
[7] S. Sergent, M. Arita, S. Kako, K. Tanabe, S. Iwamoto, and Y. Arakawa, Appl. Phys. Lett, **101**, 101106 (2012).
[8] P.R. Villeneuve and M. Piché, Phys. Rev. B **46**, 4969 (1992).
[9] CST Microwave Studio 2014 by Computer Simulation Technology, http://www.cst.com.
[10] T. Schupp, T. Meisch, B. Neuschl, M. Feneberg, K. Thonke, K. Lischka, and D.J. As, AIP Conf. Proc. **165**, 1292 (2010)
[11] G.S. Solomon, M. Pelton, and Y. Yamamoto, Phys. Rev. Lett. **86**, 3903-3906 (2001).
[12] M. Röppischer, R. Goldhahn, G. Rossbach, P. Schley, C. Cobet, N. Esser, T. Schupp, K. Lischka, and D.J. As, J. AIP **106**, 076104 (2009).
[13] M. Feneberg, M. Röppischer, C. Cobet, N. Esser, J. Schörmann, T. Schupp, D.J. As, F. Hörich, J. Bläsing, A. Krost, and R. Goldhahn, Phys. Rev. B **85**, 155207 (2012).
[14] S.G. Johnson, S. Fan, P.R. Villeneuve, J.D. Joannopoulos, and L.A. Kolodziejski, Phys. Rev. B **60**, 5751 (1999).
[15] D. Néel, S. Sergent, M. Mexis, D. Sam-Giao, T. Guillet, C. Brimont, T. Bretagnon, F. Semond, B. Gayral, S. David, X. Checoury, and P. Boucaud, Appl. Phys. Lett. **98**, 261106 (2011).